

Global environmental controls on wildfire burnt area, size and intensity

Article

Published Version

Creative Commons: Attribution 4.0 (CC-BY)

Open Access

Haas, O., Prentice, I. C. and Harrison, S. P. ORCID: <https://orcid.org/0000-0001-5687-1903> (2022) Global environmental controls on wildfire burnt area, size and intensity. *Environmental Research Letters*, 17 (6). 065004. ISSN 1748-9326 doi: 10.1088/1748-9326/ac6a69 Available at <https://centaur.reading.ac.uk/117397/>

It is advisable to refer to the publisher's version if you intend to cite from the work. See [Guidance on citing](#).

To link to this article DOI: <http://dx.doi.org/10.1088/1748-9326/ac6a69>

Publisher: Institute of Physics

All outputs in CentAUR are protected by Intellectual Property Rights law, including copyright law. Copyright and IPR is retained by the creators or other copyright holders. Terms and conditions for use of this material are defined in the [End User Agreement](#).

www.reading.ac.uk/centaur

CentAUR

Central Archive at the University of Reading

Reading's research outputs online

LETTER • OPEN ACCESS

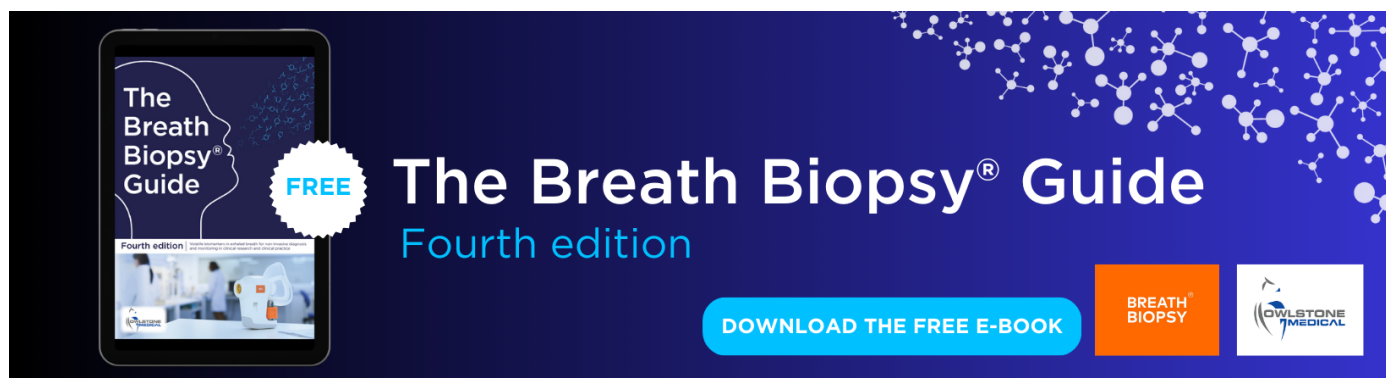
Global environmental controls on wildfire burnt area, size, and intensity

To cite this article: Olivia Haas *et al* 2022 *Environ. Res. Lett.* **17** 065004

View the [article online](#) for updates and enhancements.

You may also like

- [Projected changes in fire size from daily spread potential in Canada over the 21st century](#)
Xianli Wang, Kala Studens, Marc-André Parisien et al.
- [Projected changes in daily fire spread across Canada over the next century](#)
Xianli Wang, Marc-André Parisien, Steve W Taylor et al.
- [Human impact on wildfires varies between regions and with vegetation productivity](#)
Gitta Lasslop and Silvia Kloster



The Breath Biopsy® Guide
Fourth edition

FREE

DOWNLOAD THE FREE E-BOOK

BREATH BIOPSY

OWLSTONE MEDICAL

ENVIRONMENTAL RESEARCH
LETTERS

LETTER

Global environmental controls on wildfire burnt area, size, and intensity

OPEN ACCESS

RECEIVED
26 January 2022REVISED
5 April 2022ACCEPTED FOR PUBLICATION
26 April 2022PUBLISHED
13 May 2022

Original content from
this work may be used
under the terms of the
[Creative Commons
Attribution 4.0 licence](#).

Any further distribution
of this work must
maintain attribution to
the author(s) and the title
of the work, journal
citation and DOI.

Olivia Haas^{1,2,*}, Iain Colin Prentice^{1,2} and Sandy P Harrison^{1,3} ¹ Leverhulme Centre for Wildfires, Environment and Society, Imperial College London, South Kensington, London SW7 2BW, United Kingdom² Georgina Mace Centre for the Living Planet, Department of Life Sciences, Imperial College London, Silwood Park Campus, Buckhurst Road, Ascot SL5 7PY, United Kingdom³ Geography and Environmental Science, University of Reading, Whiteknights, Reading RG6 6AH, United Kingdom

* Author to whom any correspondence should be addressed.

E-mail: o.haas20@imperial.ac.uk**Keywords:** fire regimes, fuel loads, fire spread, landscape fragmentation, generalized linear model, vegetation modelsSupplementary material for this article is available [online](#)**Abstract**

Fire is an important influence on the global patterns of vegetation structure and composition. Wildfire is included as a distinct process in many dynamic global vegetation models but limited current understanding of fire regimes restricts these models' ability to reproduce more than the broadest geographic patterns. Here we present a statistical analysis of the global controls of remotely sensed burnt area (BA), fire size (FS), and a derived metric related to fire intensity (FI). Separate generalized linear models were fitted to observed monthly fractional BA from the Global Fire Emissions Database (GFEDv4), median FS from the Global Fire Atlas, and median fire radiative power from the MCD14ML dataset normalized by the square root of median FS. The three models were initially constructed from a common set of 16 predictors; only the strongest predictors for each model were retained in the final models. It is shown that BA is primarily driven by fuel availability and dryness; FS by conditions promoting fire spread; and FI by fractional tree cover and road density. Both BA and FS are constrained by landscape fragmentation, whereas FI is constrained by fuel moisture. Ignition sources (lightning and human population) were positively related to BA (after accounting for road density), but negatively to FI. These findings imply that the different controls on BA, FS and FI need to be considered in process-based models. They highlight the need to include measures of landscape fragmentation as well as fuel load and dryness, and to pay close attention to the controls of fire spread.

1. Introduction

Fire is a necessary component of some ecosystems, but a destructive influence in others (Keeley *et al* 2011, Archibald *et al* 2018, Harrison *et al* 2021). In both cases, however, it represents a major influence on vegetation structure and composition. Recent changes in wildfire regimes, especially the incidence of exceptionally large fires in some regions, have raised serious concerns about how they will develop in response to projected future changes in climate and land use (Bond *et al* 2005, Pausas and Keeley 2009, Pausas and Ribeiro 2017).

Wildfire regimes are characterized as combinations of specific fire properties (Krebs *et al* 2010, Archibald *et al* 2013, 2018), of which the most cited are total burnt area (BA) and the sizes and intensities of individual fires. Although all these properties are understood to be jointly controlled by climatic, vegetation and land-cover conditions (Archibald *et al* 2013, 2018, Kelley *et al* 2019, Rogers *et al* 2020), the specifics remain unclear. This is manifested in the poor performance of process-based models designed to predict wildfire and its interactions with vegetation. Fire-enabled dynamic global vegetation models (DGVMs) have been used to simulate fire during

the historical period (e.g. Teckentrup *et al* 2019), and to predict how fire regimes might change in future (Kloster *et al* 2012, Sheehan *et al* 2015, Wu *et al* 2021). However, the Fire Model Intercomparison Project (FireMIP: Hantson *et al* 2016, Rabin *et al* 2017) showed that process-based models performed no better than empirical models in predicting BA (Forkel *et al* 2019a, Hantson *et al* 2020). Furthermore, no fire-enabled DGVM could predict global patterns in fire size (FS) better than a null model that assumed the same mean size everywhere (Hantson *et al* 2020). This failure has been attributed to inadequate understanding, and therefore incomplete or incorrect representation, of the key processes and their relationship to environmental factors (Forkel *et al* 2019a, Hantson *et al* 2020) in process-based models.

Several empirical studies have investigated the relationships between environmental factors and remotely sensed BA (e.g. Bistinas *et al* 2013, 2014, Knorr *et al* 2014, 2016, Andela *et al* 2017, Forkel *et al* 2017, 2019b, Kuhn-Régner *et al* 2021). Global FS has been shown to vary along precipitation gradients, with greater aridity linked to larger fires (Hantson *et al* 2015). Human activity on the other hand strongly restricts FS through landscape fragmentation, which limits fire spread (Hantson *et al* 2015, Andela *et al* 2017, Laurent *et al* 2019). Intensity depends on fire type, with crown fires generally more intense than ground fires (Sugihara *et al* 2006, Keeley 2009, Archibald *et al* 2018). However, research into the controls of the geographic patterns in FS and fire intensity (FI) has been limited, mainly due to the lack of observations (Bowman 2018). Novel products from newly available satellite data sets (e.g. Laurent *et al* 2018, Andela *et al* 2019, Artés *et al* 2019) provide new opportunities to investigate these controls.

Four conditions must be met for a fire to start. There must be sufficient fuel; it must be dry, and therefore flammable; weather conditions must be suitable; and there must be an ignition source (Bradstock 2010). Once ignition occurs, however, other factors may influence whether the fire spreads, how rapidly it spreads, and how intense it is (Archibald *et al* 2013). In fire-enabled DGVMs, BA is sometimes derived as the product of the number of fires started and a mean FS. This concept intrinsically links ignition frequency to the total amount of burning, an assumption that has been challenged (Bistinas *et al* 2014, Harrison *et al* 2021). Globally, FI has been observed to increase with fire occurrence up to a threshold, also known as the intermediate fire occurrence-intensity (IFOI) hypothesis (Pausas and Ribeiro 2013, Luo *et al* 2017). In process-based models FS is often dependent on FI, defined as the amount of energy released by a wildfire, through rate-of-spread equations (Yue *et al* 2014, Hantson *et al* 2016). Indeed, as a key component of the Rothermel equation (Rothermel 1972), greater FI is assumed to increase the speed of fire spread, thus

producing larger fires. However, this relationship has been shown to saturate in much of the world (Laurent *et al* 2019).

In this paper, we explored the causal relationships between environmental factors and geographic variation in fractional BA, FS and FI. These underlying relationships may differ from the emergent relationships with individual drivers. We develop generalized linear models (GLMs) for each fire property, using a common set of quantitative predictors representing vegetation, land cover, climate, and ignition sources. We explore the direction and power of the linear relationships fitted between each predictor and each fire property, when all other variables are held constant, to identify significant drivers and constraints for different aspects of the fire regime and assess their (differing) relative importance.

2. Data and methods

2.1. Fire data

BA data were derived from monthly mean fractional BA from the Global Fire Emissions Database (GFEDv4; Randerson *et al* 2018). This provides monthly BA at $0.25^\circ \times 0.25^\circ$ resolution for the period from June 1995 to December 2016. FS was represented by median monthly FS from the Global Fire Atlas (Andela *et al* 2019). This provides global vector shapefiles gridded at 500 m with the timing and location of each individual fire, along with its key properties, from 2003 to 2016. The median was used to account for the highly skewed distribution of FS. FI was approximated by a metric based on the median monthly fire radiative power (FRP) in the MCD14ML dataset (Giglio *et al* 2006). This provides geographic coordinates of active $\sim 1 \text{ km} \times 1 \text{ km}$ fire pixels detected by the Moderate Resolution Imaging Spectroradiometer (MODIS) sensor onboard the Terra and Aqua satellites, from 2000 to 2017. FRP in megawatt (MW) is provided for each pixel. Only type 0 pixels (presumed vegetation fires) and with confidence $>50\%$ were retained. We divided the monthly median values by the square root of monthly median FS in the Global Fire Atlas. Although FRP has been used directly to indicate FI (Wooster and Zhang 2004, Wooster *et al* 2005), it is a measure of the instantaneous energy emission over the whole pixel. Normalizing by the square root of median FS provides a measure (in units of W m^{-1}) more closely related to the fireline intensity of any given fire (see supplementary II available online at stacks.iop.org/ERL/17/065004/mmedia).

2.2. Predictor variables

A set of predictors representing vegetation, land cover, climate and ignition sources was identified from previous research on the drivers of wildfire regimes globally (Bistinas *et al* 2014, Forkel *et al* 2018, 2019b).

2.2.1. Vegetation, land cover and landscape fragmentation

Mean annual gross primary production (GPP) obtained from monthly outputs of the P-model (Stocker *et al* 2020), a first-principles model of GPP that allows continuous acclimation of photosynthetic parameters to environmental variations in space and time (supplementary III), was used as an index of vegetation productivity. Land cover categories were used to represent vegetation types. Annual fractional shrubland, grassland and tree cover were obtained by converting the land cover types from the European Space Agency (ESA) Climate Change Initiative (CCI) Land Cover dataset, which provides annual maps from 1992 to 2015 (Li *et al* 2018), to fractional cover following Poulter *et al* (2015) using the conversion table in Forkel *et al* (2017). Landscape fragmentation was represented by cropland cover, two landscape heterogeneity indexes and road density. This categorization is by no means exhaustive, however all three of these factors have been shown to influence fire activity and spread (Pfeiffer *et al* 2013, Andela *et al* 2017, Povak *et al* 2018, Kelley *et al* 2019, Harrison *et al* 2021, Pausas and Keeley 2021). Vector ruggedness measure (VRM) and topographic position index (TPI) were used to represent topographic controls (Sappington *et al* 2007). VRM captures variability in slope and aspect into a single measure, providing a measure for terrain heterogeneity, whilst TPI provides information on valleys (negative values) and ridges (positive values). We obtained 50 km aggregated information for these variables, derived from the digital elevation model products of global 250 m GMTED2010 and near-global 90 m SRTM4.1dev (Amatulli *et al* 2018). Although the data layers only cover 2010, it was assumed that there would be no significant changes in VRM or TPI from 2010 to 2015 at this resolution. Fractional annual cropland cover was taken from version 3.2 of the HistorY Database of the global Environment (HYDE 3.2: Klein Goldewijk *et al* 2017) database, which provides annual data from 2000 to 2017 at $0.25^\circ \times 0.25^\circ$ resolution. Road density was obtained from the Global Roads Inventory Project (GRIP) database (Meijer *et al* 2018), which provides average road density from 1979 to 2015 (although >50% of the data is from 2010 or later) at $0.5^\circ \times 0.5^\circ$ resolution.

2.2.2. Climate

We calculated the total monthly number of dry days (DDs), monthly mean daily vapour pressure deficit (VPD), monthly mean daily diurnal temperature range (DTR) and monthly mean wind speed from the WFDE5 bias-adjusted ERA5 dataset (Cucchi *et al* 2020) (supplementary I). This provides hourly data from 1979 to 2018 at $0.5^\circ \times 0.5^\circ$ resolution.

2.2.3. Ignition sources

Annual values of population density, representing the potential for human ignitions, were taken from HYDE3.2. Mean monthly lightning ground-strike density, representing potential natural ignitions, was obtained from the worldwide lightning location network (WWLLN) Global Lightning Climatology (WGLC) dataset (Kaplan and Lau 2021). This contains global monthly gridded data at $0.5^\circ \times 0.5^\circ$ resolution from 2010 to 2020.

2.3. Data processing

A seasonal climatology over the common 6 years period from 2010 to 2015 was constructed for all variables with monthly data, eliminating inter-annual variability. This was the only common period for all the variables but, given the strong spatial patterns involved, we assume this is sufficiently long for our purpose. Annual variables were averaged over the 6 years. For monthly data, a single global layer was constructed from the seasonal climatology. For each grid cell, the value of the month with (on average) the maximum number of DD, the largest DTR, and the highest VPD were selected. Wind speed value was taken from the hottest month of the year (determined from the WFDE5 2 m air temperature (Cucchi *et al* 2020)). For lightning, the mean value over the seasonal climatology was selected.

Additionally, we included two seasonality predictors to account for periods of high vs low productivity (seasonality of GPP) and wet vs dry seasons (seasonality of DD). These seasonality predictors were constructed from the GPP and DD climatology, respectively. To capture the seasonality of GPP, we divided the range of monthly values from the seasonal climatology by the mean value of all 12 months. The same was done to capture the seasonality of DD. For road density and the VRM, no additional processing was performed. This provided a set of 16 predictors (table 1). For the fire variables, the mean value over the seasonal climatology was selected. All variables were re-gridded to a $0.5^\circ \times 0.5^\circ$ resolution grid to order to be compatible with the lowest resolution datasets and all analysis were conducted at this scale.

Predictor variables were transformed appropriately (table 1) to reduce differences in scale and improve interpretability (Schielzeth 2010). GPP was the only predictor with zero values. We applied logarithmic transformation to GPP, ignoring zero values in the model. Since we assume no fire occurs where GPP was zero, the missing values were re-coded as zero afterwards. Square root transformation was applied to predictors representing densities, for which zero values were assumed to be meaningful. To reduce distortion introduced by a few (extremely rare) very large values, FS and intensity were transformed to z-scores:

Table 1. Summary of predictor and fire response variables.

Predictors	Data source	Abbreviation	Transformation
Vegetation, land cover and landscape fragmentation			
Annual gross primary production ($\text{g C m}^{-2} \text{a}^{-1}$)	P-model (Stocker <i>et al</i> 2020)	GPP	Logarithmic
Gross primary production seasonality (unitless)	P-model (Stocker <i>et al</i> 2020)	GPP_seasonality	Logarithmic
Fractional shrubland cover	ESA CCI Landcover	Shrub	None
Fractional grassland cover	ESA CCI Landcover	Grass	None
Fractional tree cover	ESA CCI Landcover	Tree	None
Road density (km^{-2})	GRIP (Meijer <i>et al</i> 2018)	Roads	Square root
Fractional cropland cover	HYDE 3.2 (Klein Goldewijk <i>et al</i> 2017)	Crop	None
Vector ruggedness measure	(Amatulli <i>et al</i> 2018)	VRM	None
Topographic position index	(Amatulli <i>et al</i> 2018)	TPI	None
Climate			
Maximum monthly number of dry days	WFDE5 (Cucchi <i>et al</i> 2020)	DD	Logarithmic
Seasonality of monthly number of dry days (unitless)	WFDE5 (Cucchi <i>et al</i> 2020)	DD_seasonality	Logarithmic
Maximum mean monthly vapour pressure deficit (Pa)	WFDE5 (Cucchi <i>et al</i> 2020)	VPD	Logarithmic
Maximum mean monthly diurnal temperature range (K)	WFDE5 (Cucchi <i>et al</i> 2020)	DTR	Logarithmic
Mean wind speed of the hottest month (m s^{-1})	WFDE5 (Cucchi <i>et al</i> 2020)	Wind	Logarithmic
Ignition sources			
Population density (km^{-2})	HYDE 3.2 (Klein Goldewijk <i>et al</i> 2017)	Popd	Square-root
Mean monthly lightning ground-strikes (km^{-2})	WGLC WWLLN (Kaplan <i>et al</i> 2021)	Light	Square-root
Fire variables			
Monthly mean burnt area (fraction)	GFEDv4 (Randerson <i>et al</i> 2018)	BA	None (logit link function)
Monthly median fire size (km^2)	Global Fire Atlas (Andela <i>et al</i> 2019)	FS	Min–max normalized (log link function)
Monthly median fire intensity (W km^{-1})	MCD14ML (Giglio <i>et al</i> 2006)	FI	Median FRP divided by square root of median FS, min–max normalized (log link function).

$$z_i = (x_i - \mu_i) / \sigma_i \quad (1)$$

where μ_i is the mean and σ_i is the standard deviation of the variable x_i , and values of x_i yielding z -scores >3 or <-3 were excluded (Shiffler 1988). The remaining values were scaled using the min–max transformation:

$$x_{ni} = [x_i - \min(x_i)] / [\max(x_i) - \min(x_i)]. \quad (2)$$

To confine the range of the transformed (x_{ni}) values to the interval (0, 1). This scaling helps interpretability but does not interfere with the statistical distribution of values (Juszczak *et al* 2002).

2.4. Statistical modelling

GLMs have previously been used to model BA (Lehsten *et al* 2010, Bistinas *et al* 2014) because

they provide highly interpretable results (Nelder and Wedderburn 1972, McCullagh and Nelder 1989). GLMs are useful because they (a) handle response variables with highly non-Gaussian error distributions without the problems introduced e.g. by log-transformation of response variables, (b) are embedded in a well-established (multiple regression) framework, which allows quantification of the independent effects of multiple predictors even if they are partially correlated with one another, and (c) generate partial residual plots showing the effect of each predictor while the others are held constant (Larsen and McCleary 1972). The relative importance of each predictor was assessed using absolute t -values (the fitted regression coefficient of each predictor divided by its standard error) calculated with the package *caret* in R. These t -values are unitless and scale-invariant,

and in addition to providing a simple measure of the importance of each predictor (Grömping 2015), are directly related to the coefficient of determination (R^2): the squared t -value of each predictor x_i represents the reduction in R^2 that occurs when that predictor is removed from the model (Darlington 1968, Bring 1996). Thus, the larger the t -value of a predictor, the more variance it explains. Variance inflation factors (VIFs) were examined to evaluate multicollinearity among predictors. A VIF of 1 indicates no collinearity; we eliminated predictors with VIF values >5 (O'Brien 2007). We used normalized mean error (NME) to evaluate the performance of the models, following Kelley *et al* (2013). NME is a standard metric to assess global fire model performances, allowing direct comparison with these other models (Kelley *et al* 2019, Hantson *et al* 2020). NME is defined as:

$$\text{NME} = \frac{\sum A_i |\text{obs}_i - \text{sim}_i|}{\sum A_i |\text{obs}_i - \overline{\text{obs}}|}$$

where the difference between observations (obs) and simulation (sim) are summed over all cells (i) weighted by cell area (A_i) and normalized by the average distance from the mean of the observations (obs). An NME score has no upper limit, but smaller values signify better performance with a zero-value meaning perfect fit between observed and simulated values. All analysis were conducted in R using the stats, car, benchmarkMetrics and visreg packages.

Fractional BA was equated with the probability of burning, ranging between 0 and 1. We assumed this probability to follow a quasi-binomial distribution, and applied the logit link function. The distribution of FS and intensity is hypothesized to follow a power law (Kumar *et al* 2011, Hantson *et al* 2016). We assumed a quasi-Poisson distribution for both variables (due to their large overdispersion, with many very small values) and applied the log link function.

All three models were initially constructed using all 16 predictors (see supplementary IV). Population density has been hypothesized to indicate landscape fragmentation (Bistinas *et al* 2014, Knorr *et al* 2014) but is highly correlated with road density ($r = 0.31$). Therefore, we made two additional model runs, with all predictor variables excluding either population density or road density, to assess how much of the variance was explained by these predictors when the other is not present (see supplementary V). VPD, the absolute difference in water vapour content of the air and the water holding capacity of the atmosphere, influences long-term plant growth and photosynthesis (Park Williams *et al* 2013, Abatzoglou *et al* 2016, Grossiord *et al* 2020) but GPP seasonality is correlated with VPD ($r = 0.71$). We therefore made two separate model runs, using all predictors but excluding either GPP seasonality or VPD (see supplementary VI). From these runs, we present the best model

for each fire property. Only predictors with $p < 10^{-5}$ were retained, resulting in three final models that includes only predictors with substantial explanatory power.

3. Results

All 16 predictors showed significant relationships with BA (table S2). GPP ($t = 63.00$), DD ($t = 70.23$) and DD seasonality ($t = 59.26$), grassland cover ($t = 52.91$), and VPD ($t = 39.11$) showed strong positive relationships with BA (figure 1). Shrubland cover ($t = 26.35$), DTR ($t = 19.82$) and TPI ($t = 18.86$) also showed positive relationships with BA. Lightning ($t = 12.35$) and population density ($t = 10.64$) showed positive relationships with BA (the relationship with population density however became negative when road density was excluded). Road density ($t = -37.32$), VRM ($t = -21.39$), tree cover ($t = -18.74$), cropland ($t = -10.05$) and wind ($t = -6.80$) and showed negative relationships with BA (figure 1).

Eleven of the original 16 predictors were retained in the final FS model (table 2). GPP, grassland cover, TPI and population density were statistically insignificant, and seasonality of DD did not meet the t -value threshold (table S2). DTR ($t = 14.46$), and wind speed ($t = 14.41$), followed in importance by DD ($t = 11.16$), shrubland cover ($t = 7.61$), lightning ($t = 5.50$) GPP seasonality ($t = 5.18$) and VPD ($t = 5.12$) all showed positive relations with FS (figure 1). Cropland cover ($t = -22.42$), road density ($t = -16.47$), VRM ($t = 5.78$) and tree cover ($t = -5.25$) showed negative relationships with FS (figure 1).

Only nine of the original 16 predictors were retained in the final model for FI (table 2). DTR, wind speed cropland cover and TPI were statistically insignificant and VRM and seasonality of GPP did not meet the t -value threshold (table S2). Tree cover ($t = 9.08$) and road density ($t = 8.58$) showed positive relationships with FI, whereas VPD ($t = -47.55$), GPP ($t = -18.47$), DD ($t = -16.18$) and DD seasonality ($t = -14.27$) population density ($t = -13.49$) and lightning ($t = -7.15$) all showed negative relationships (figure 1).

Excluding population density did not change the significance or sign of any relationship with BA, FS or FI. Excluding road density led to a weak ($p = 0.05$) negative relationship between population density and BA, a highly significant negative relationship with FS, but no change for FI (table S3). Excluding VPD lead the seasonality of GPP to become insignificant with BA and to exhibit a weak ($p = 0.06$) positive relationship with FS. For FI, the exclusion of VPD lead to a large increase in the strength of the seasonality of GPP (from $t = 3.32$ to $t = 27.67$) (table S4).

The strongest relationships differed between models. BA was driven above all by variables related

Table 2. Summary statistics with regression coefficients, *t*-values, and VIFs for each of the final models. Predictors included were all significant at $t > 4.5$ ($p < 10^{-5}$).

Predictors	Burnt area (BA)			Fire size (FS)			Fire intensity (FI)		
	Coefficient	<i>t</i> -value	VIF	Coefficient	<i>t</i> -value	VIF	Coefficient	<i>t</i> -value	VIF
(Intercept)	−48.25	−103.6	—	−13.09	−25.75	—	6.43	44.85	—
GPP ($\text{g C m}^{-2} \text{ a}^{-1}$)	1.76	63.00	4.13	—	—	—	−0.21	−18.47	3.04
Seasonality of GPP	0.59	14.78	2.43	0.30	5.18	3.29	—	—	—
Fractional tree cover	−0.93	−18.74	2.92	−0.42	−5.25	2.19	0.19	9.08	2.20
Fractional shrubland cover	1.39	26.35	1.70	0.64	7.61	1.29	—	—	—
Fractional grassland cover	2.93	52.91	1.56	—	—	—	−0.35	−11.91	1.18
Road density (km^{-2})	−0.05	−37.32	1.44	−0.04	−16.47	1.40	0.00	8.58	1.80
Fractional cropland cover	−0.79	−10.05	2.15	−3.51	−22.42	1.42	—	—	—
VRM	−188.70	−21.39	1.55	−62.28	−5.78	1.50	—	—	—
TPI	0.43	18.86	1.33	—	—	—	—	—	—
Maximum monthly number of DDs	4.54	70.23	2.89	1.14	11.16	2.30	−0.31	−14.27	1.95
Seasonality of monthly number of DDs	1.33	59.26	2.57	—	—	—	−0.15	−16.18	1.97
Maximum mean monthly VPD (Pa)	1.35	39.11	1.78	0.31	5.12	3.72	−0.66	−47.55	2.03
Maximum mean monthly DTR (K)	0.87	19.82	1.78	1.24	14.46	1.91	—	—	—
Mean wind speed of the hottest month (m s^{-1})	−0.20	−6.80	1.93	0.80	14.41	2.20	—	—	—
Mean monthly lightning ground-strikes (km^{-2})	0.94	12.35	1.66	0.83	5.50	2.06	−0.30	−7.15	2.11
Population density (km^{-2})	0.02	10.64	1.71	—	—	—	−0.01	−13.49	1.56
R^2 (McFadden 1974)	0.69			0.29			0.27		

to fuel availability (GPP and grass cover: positive relationships) and dryness (DD and the seasonality of DD: positive relationships) (figure 2). Cropland cover and road density (negative relationships) were the two strongest drivers of FS (positive relationships), followed closely by DTR and wind speed (positive relationships) (figure 2). VPD and GPP showed the strongest relationships with FI (figure 2), both being negative relationships.

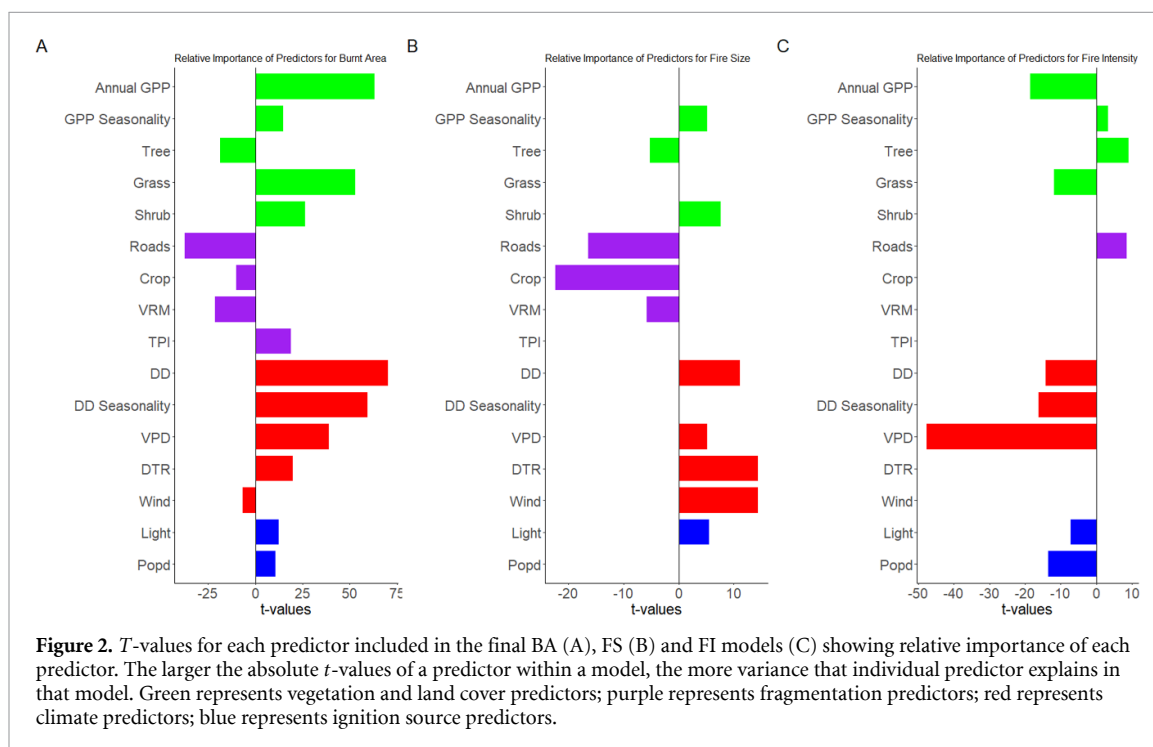
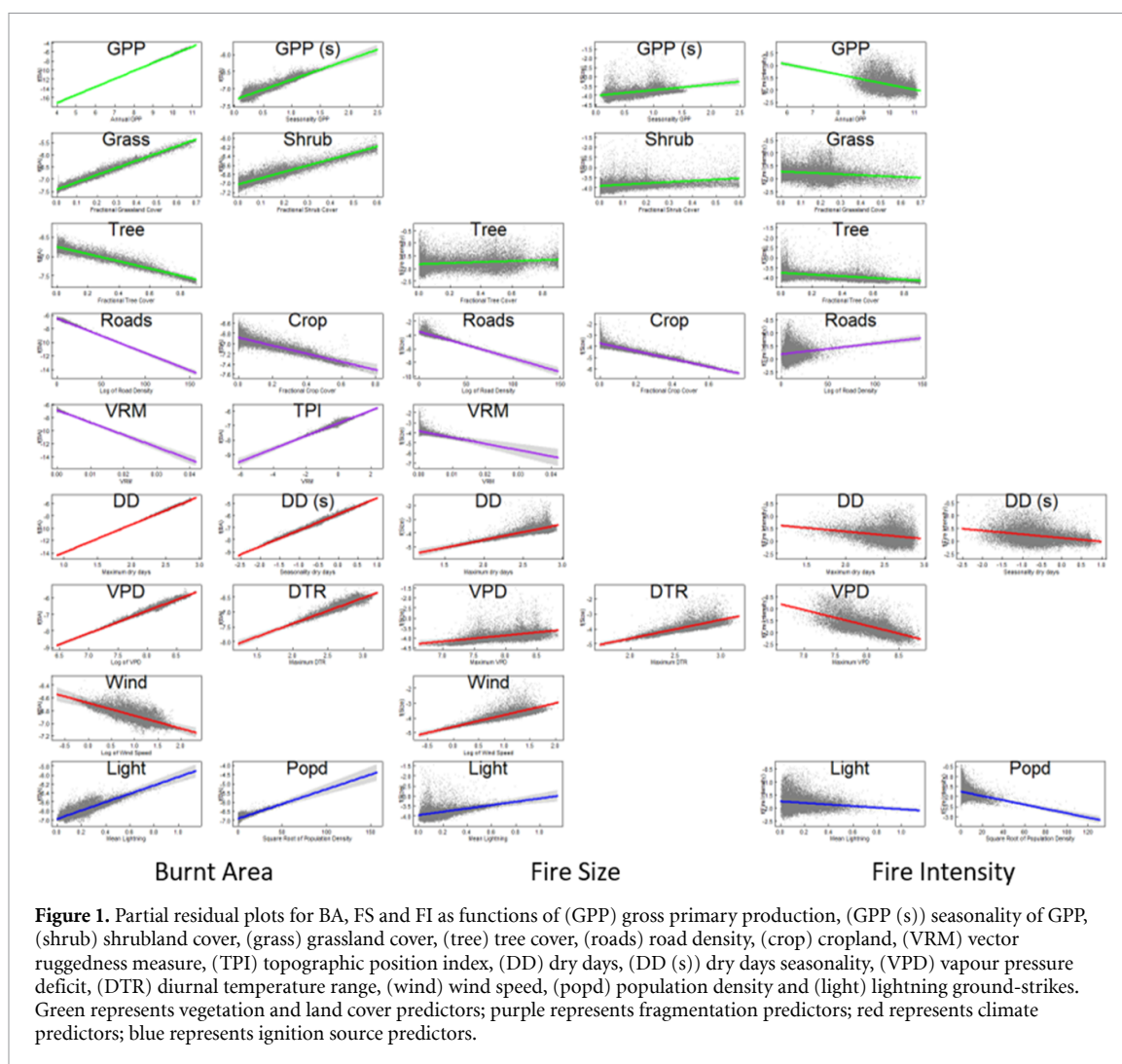
The predictive power of the BA model ($R^2 = 0.69$) was substantially greater than that for FS ($R^2 = 0.29$) or FI ($R^2 = 0.27$), suggesting these last two properties are influenced by factors not included in the analysis. Despite modest R^2 values, however, all three models capture the broad geographic patterns of the observations (figure 3). We obtained NME scores of 0.51, 0.86 and 0.86 for the BA, FS and FI models, respectively. Our BA and FS models outperformed all models included in the Fire Intercomparison Project, which had NME scores ranging from 0.60 to 1.10 for BA and 0.96–0.98 for FS (Hantson *et al* 2020). Although no direct comparison with the FireMIP models is possible for FI, this model performed as well as the FS model. All three models perform better than a null mean model, which assumes the observational mean globally and produces an NME score of 1. All three GLMs tend to compress the reconstructed range of values, leading to apparent over- (under-) prediction at the low (high) extremes. However, the partial

residual plots (figure 1) do not show systematic biases suggesting that the apparent compression may simply reflect the highly stochastic nature of wildfire. The fitted models represent an estimate of the most probable outcome, whereas the observations are what actually happened—including some exceptionally large and/or intense fires, but also many grid cells where no fires were detected. The observations also have a systematic low-end bias, as fires smaller than a certain size are not detected by MODIS (Rotera *et al* 2019, Ramo *et al* 2021).

4. Discussion

We have shown that the environmental controls on geographic patterns of BA, FS and FI are different. Here we discuss these differences, how they might be interpreted, and their implications for improving predictive models.

BA was shown to be primarily driven by fuel availability (represented by GPP and grass cover) and dryness (particularly DD, but also VPD and DTR) and constrained by road density. These results are consistent with previous research (Bistinas *et al* 2014, Andela *et al* 2017, Forkel *et al* 2019a, 2019b, Kelley *et al* 2019, Kuhn-Régnier *et al* 2021) and with the IFOI hypothesis that the main drivers of fire activity are fuel availability and fire weather, varying in importance globally along the productivity gradient



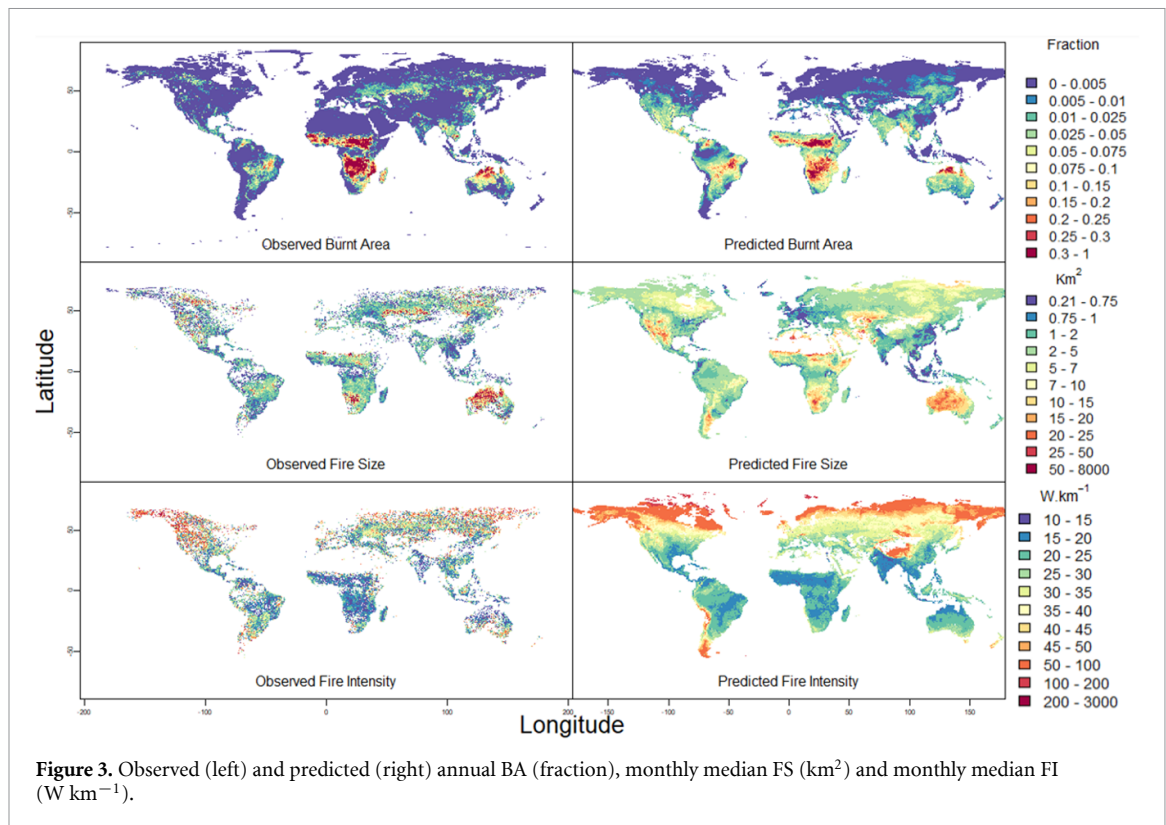


Figure 3. Observed (left) and predicted (right) annual BA (fraction), monthly median FS (km²) and monthly median FI (W km⁻¹).

(Pausas and Ribeiro 2013). In addition, both lightning and population density positively influence BA. The apparent fire-suppressing effect of population density (noted by Bistinas *et al* 2014, Knorr *et al* 2014, among others) is represented in our analysis by road density. Roads provide barriers to fire spread, hence the negative relationship of BA to road density. When this effect is accounted for, population density relates positively to BA. The positive relationship with TPI suggests that fractional BA increases as we move from valleys to ridges, and that ridges do not constrain BA. This result is in line with previous research suggesting that ridges do not necessarily provide fire breaks, and that valleys, characterized by higher soil moisture, lower insolation, and higher terrain shading exhibit stronger control on fire spread (Povak *et al* 2018). Terrain heterogeneity (VRM) however, strongly constrains BA. Although wind speed promotes fire spread, wind speed was negatively related to BA, in line with previous research showing the limited effect of wind speeds on BA at a coarse global scale (Lasslop *et al* 2015).

Factors promoting fire spread, namely wind speed and dryness (particularly DTR, but also VPD) were shown to be the primary drivers of FS while cropland cover, road density, and terrain heterogeneity (VRM), all agents of landscape fragmentation, strongly constrain FS. The effect of wind speed was significant for FS. TPI was not statistically significant, suggesting that the presence of steep slopes and ridges do not necessarily control fire spread (Povak *et al* 2018). This

is consistent with research suggesting fuel continuity is important for FS (Viedma *et al* 2009, Hantson *et al* 2015, Laurent *et al* 2019). In contrast with BA, FS showed no significant relationship to GPP or grassland cover—indicating fuel availability is less important for FS than BA, and that large fires tend not to occur in highly productive environments.

The FI metric was shown to be positively influenced by tree cover and road density and constrained by dryness (particularly VPD, and also DD). Lack of precipitation has been shown to limit fuel build-up (Keeley and Syphard 2017, Kuhn-Régner *et al* 2021, Pausas and Keeley 2021) and high atmospheric dryness (VPD) limits plant growth (Fu *et al* 2022). The negative relationship with dryness is therefore not surprising since we expect fuel load to be an important driver of FI. Although GPP is negatively related to the FI measure, when VPD was excluded, the seasonality of GPP became the strongest driver of the FI model, an effect that did not translate into the other two models. This would suggest that sufficient atmospheric moisture along with seasonal changes in productivity, provide the dense fuel loads necessary for intense fires. These dense fuel loads are mostly restricted to areas with high tree cover, explaining the negative relationship with grassland and shrubland cover (Archibald *et al* 2013, Luo *et al* 2017, Archibald *et al* 2018). The overall negative relationship with GPP could therefore be explained by intense fires mainly occurring in regions with a seasonal variation in productivity, more characteristic of the high latitude

forests than the more productive, tropical ones. A plausible reason for the positive relationship between FI and road density is the correlation between intense deforestation fires and the access roads required in remote forest areas. The observed negative relationship between lightning and FI is expected since frequent fire limits fuel build-up (Pausas and Ribeiro 2013, Luo *et al* 2017). Similarly, the negative relationship between population density and FI can be interpreted as a trade-off between the frequency and intensity of fires, probably compounded by active fire suppression in densely populated regions.

The FI metric shared few strong predictors with either of the other models. It was not limited by landscape fragmentation; wind speed and DTR were insignificant, and it showed an opposite relationship with dryness to the other models. This implies that the widely assumed positive relationship between FI and FS does not hold generally. Saturation of this relationship in fire-prone ecosystems (Laurent *et al* 2019) has been attributed to feedback between BA and fuel connectivity, with landscape fragmentation increasing through the fire season due to previous burns, thus limiting FS. Our results are consistent with this but suggest additional factors may influence the relationship between FS and intensity. The limiting effect of dryness on FI suggests fuel loads are important, consistent with previous research (Forkel *et al* 2019a, Kuhn-Régner *et al* 2021). Antecedent conditions and current dryness may promote fine and flammable fuels that favour large but cooler fires, while limiting build-up of the larger, more dense fuels required for intense fires (Hantson *et al* 2015, Kuhn-Régner *et al* 2021).

Some of the original 16 predictors proved unimportant for the FS and FI models. Although all predictors included in the final models were highly significant ($p < 10^{-5}$) the partial residual plots suggest that there may be cases where the relationship is not linear (e.g. GPP), although in no case did the inclusion of a non-linear (polynomial) term in the models improve predictability. Together with the relatively low level of predictability of these two models, this suggests that other factors need to be investigated. There is growing evidence of fire regimes differing in similar biomes, as well as different biomes showing similar fire regimes—phenomena that cannot be explained without consideration of fire-adaptive plant traits (Hollingsworth *et al* 2013, Pausas 2015, Pausas *et al* 2016, Pausas and Ribeiro 2017, Archibald *et al* 2018). The boreal forests in North America and Eurasia are a case in point, where crown and surface fires respectively are dominant (Wooster and Zhang 2004, Wirth 2005, Sitnov and Mokhov 2018). The distribution of fire-adaptive plant traits may be crucial to understand FS and intensity (Harrison *et al* 2021). Unfortunately, although there is information about fire-adaptive traits for some regions, including southern Europe and eastern Australia (Tavşanoğlu and Pausas

2018, Falster *et al* 2021), such information is limited elsewhere; this is a key data gap.

Our results have implications for fire modelling. Process-based models generally rely on the product of fire counts and FS to simulate BA. Our results suggest that the controls on BA, FS and FI should be modelled separately. Our results also add to the growing literature suggesting the use of population density to determine number of ignitions should be reviewed (Bistinas *et al* 2014, Knorr *et al* 2014, 2016, Andela *et al* 2017). Our results suggest it would be better to include landscape fragmentation explicitly as a control on fire spread. Population density apparently has a globally negative effect on BA unless an alternative measure of landscape fragmentation, such as road density, is included (table S3). Thus, population density as used in current models is a surrogate for human fire suppression and landscape fragmentation (Bistinas *et al* 2013, Knorr *et al* 2014, 2016, Harrison *et al* 2021); any positive impact of population on ignitions will only be captured when fragmentation is explicitly considered. Some process-based models account for the emergent relationship between population and fire properties (Harrison *et al* 2021), whereby increasing population density leads to increased ignitions up to a threshold and further increases lead to suppression (Rabin *et al* 2017). We have shown that some elements of landscape fragmentation exhibit strong spatial control on fire spread that can be modelled at a global scale. In addition to factors of landscape fragmentation considered here, additional features such as deforestation, non-flammable land cover and previous burns can all fragment the landscape and thus effect fuel continuity (Laurent *et al* 2019, Harrison *et al* 2021, Pausas and Keeley 2021). There is a pressing need to investigate how each of these features of landscape fragmentation influence different aspects of the fire regime and integrate them to global wildfire modelling explicitly. Although lightning showed a positive relationship with BA and FS, the relationship was not particularly strong. Lightning also constrained FI, possibly via a trade-off between intensity and frequency. Process-based models may therefore have overestimated the importance of ignition sources generally. Indeed, fire-enabled DGVMs struggle to simulate fire starts accurately (Forkel *et al* 2019a).

We have represented FS using data from the Global Fire Atlas and intensity with FRP values from MCD14ML dataset. The Global Fire Atlas relies on the MODIS sensor, so the minimum size of a recorded fire is one MODIS pixel (0.21 km²) and thus our data does not include fires smaller than this. However, the environmental drivers of small fires are not expected to differ from those of larger fires. Although FRP has been used as a measure of FI, it represents the radiative energy emitted and does not account for convection and conduction. FI in the Rothermel equation represents the intensity of the flaming front

of an individual fire, whereas retrieved FRP values from MCD14ML integrate radiative energy over a $1 \text{ km} \times 1 \text{ km}$ pixel. The normalization introduced here provides a partial solution to this problem and accurately highlights the regions of high FI. However, work is required to derive fireline intensity more reliably from remotely sensed products.

This analysis did not account for any inter-annual variability, such as changes in the length of the fire season or a departure the established fire regime within a given year. Though these factors have been shown to influence the different aspects of the fire regime (Pausas 2004, Pausas and Keeley 2021), we were interested in the underlying climatic, land cover and ignition spatial controls when the effect inter-annual variability was removed. Understanding these controls for different aspects of the fire regime is a first and crucial step to predicting how they will respond to different conditions between years and in the future. The timeframe of this analysis was relatively short, though similar to timeframes used in previous empirical analyses due to similar data availability issues. The strong spatial patterns displayed both by the fire variables and the predictors meant that key relationships could nonetheless be established. Each model reproduces the spatial patterns of regions of high BA, large FS and high FI, allowing useful conclusions to be drawn.

Data availability statements

All predictor variables are available using the references given in tables 1 and S1. The GFEDv4 data are available at https://daac.ornl.gov/VEGETATION/guides/fire_emissions_v4.html. The Global Fire Atlas data is available at www.globalfiredata.org/fireatlas.html. The MCD14ML dataset is available at <https://earthdata.nasa.gov/earth-observation-data/near-real-time/firms/mcd14ml>.

The data that support the findings of this study are openly available at the following URL/DOI: <https://figshare.com/s/54af266b692e1d3b2316>.

Acknowledgments

O H acknowledges support from the NERC Centre for Doctoral Training in Quantitative and Modelling skills in Ecology and Evolution (Grant No. NE/S007415/1) and from the Leverhulme Trust through the Leverhulme Centre for Wildfires, Environment and Society (Grant No. RC-2018-023). S P H acknowledges support from the ERC-funded project GC2.0 (Global Change 2.0: Unlocking the past for a clearer future, Grant No. 694481) and from the Leverhulme Centre for Wildfires, Environments and Society. I C P acknowledges support from the ERC-funded project REALM (Re-inventing Ecosystem And Land-surface Models, Grant No. 787203)

and from the Leverhulme Centre for Wildfires, Environments and Society. This work is a contribution to the LEMONTREE (Land Ecosystem Models based On New Theory, observations and Experiments) project, funded through the generosity of Eric and Wendy Schmidt by recommendation of the Schmidt Futures program (S P H, I C P). We thank Martin Wooster for discussion of FRP, Alexander Kuhn-Regnier and Michel Valette for sharing data and data processing scripts, and Keith Bloomfield, Ning Dong, David Orme and David Sandoval Calle for their assistance with data problems.

Author contributions

Concepts, strategy and interpretation were developed by O H, I C P and S P H jointly. O H performed the data curation, processing and analysis, and produced the graphics and Tables. O H wrote the original draft; S P H and I C P reviewed and edited it.

Conflict of interest

The authors declare that they have no conflict of interest.

ORCID iD

Sandy P Harrison  <https://orcid.org/0000-0001-5687-1903>

References

- Abatzoglou J T, Kolden C A, Balch J K and Bradley B A 2016 Controls on interannual variability in lightning-caused fire activity in the western US *Environ. Res. Lett.* **11** 045005
- Amatulli G, Domisch S, Tuanmu M N, Parmentier B, Ranipeta A, Malczyk J and Jetz W 2018 A suite of global, cross-scale topographic variables for environmental and biodiversity modeling *Sci. Data* **5** 1–15
- Andela N, Morton D C, Giglio L, Chen Y, van der Werf G R, Kasibhatla P S, DeFries R S, Collatz G J, Hantson S and Kloster S 2017 A human-driven decline in global burned area *Science* **356** 1356–62
- Andela N, Morton D C, Giglio L, Paugam R, Chen Y, Hantson S, van der Werf G R and Randerson J T 2019 The Global Fire Atlas of individual fire size, duration, speed and direction *Earth Syst. Sci. Data* **11** 529–52
- Archibald S *et al* 2018 Biological and geophysical feedbacks with fire in the Earth system *Environ. Res. Lett.* **13** 033003
- Archibald S, Lehmann C E R, Gómez-Dans J L and Bradstock R A 2013 Defining pyromes and global syndromes of fire regimes *Proc. Natl Acad. Sci. USA* **110** 6442–7
- Artés T, Oom D, de Rigo D, Durrant T H, Maiani P, Libertà G and San-Miguel-Ayán J 2019 A global wildfire dataset for the analysis of fire regimes and fire behaviour *Sci. Data* **6** 1–11
- Bistinas I, Harrison S P, Prentice I C and Pereira J M C 2014 Causal relationships versus emergent patterns in the global controls of fire frequency *Biogeosciences* **11** 5087–101
- Bistinas I, Oom D, Sá A C L, Harrison S P, Prentice I C and Pereira J M C 2013 Relationships between human population density and burned area at continental and global scales *PLoS One* **8** e81188
- Bond W J, Woodward F I and Midgley G F 2005 The global distribution of ecosystems in a world without fire *New Phytol.* **165** 525–38

- Bowman D 2018 Wildfire science is at a loss for comprehensive data *Nature* **560** 7–8
- Bradstock R A 2010 A biogeographic model of fire regimes in Australia: current and future implications *Glob. Ecol. Biogeogr.* **19** 145–58
- Bring J 1996 A geometric approach to compare variables in a regression model *Am. Stat.* **50** 57–62
- Cucchi M, Weedon G P, Amici A, Bellouin N, Lange S, Müller Schmied H, Hersbach H and Buontempo C 2020 WFDE5: bias-adjusted ERA5 reanalysis data for impact studies *Earth Syst. Sci. Data* **12** 2097–120
- Darlington R B 1968 Multiple regression in psychological research and practice *Psychol. Bull.* **69** 161
- Falster D, Gallagher R, Wenk E H, Wright I J, Indarto D, Andrew S C, Baxter C, Lawson J, Allen S and Fuchs A 2021 AusTraits, a curated plant trait database for the Australian flora *Sci. Data* **8** 1–20
- Forkel M et al 2018 Emergent relationships on burned area in global satellite observations and fire-enabled vegetation models *Biogeosci. Discuss.* 1–31
- Forkel M et al 2019a Emergent relationships with respect to burned area in global satellite observations and fire-enabled vegetation models *Biogeosciences* **16** 57–76
- Forkel M, Dorigo W, Lasslop G, Chuvieco E, Hantson S, Heil A, Teubner I, Thonicke K and Harrison S P 2019b Recent global and regional trends in burned area and their compensating environmental controls *Environ. Res. Commun.* **1** 051005
- Forkel M, Dorigo W, Lasslop G, Teubner I, Chuvieco E and Thonicke K 2017 A data-driven approach to identify controls on global fire activity from satellite and climate observations (SOFIA V1) *Geosci. Model Dev.* **10** 4443–76
- Fu Z et al 2022 Atmospheric dryness reduces photosynthesis along a large range of soil water deficits *Nat. Commun.* **13** 1–10
- Giglio L, Csizsar I and Justice C O 2006 Global distribution and seasonality of active fires as observed with the Terra and Aqua moderate resolution imaging spectroradiometer (MODIS) sensors *J. Geophys. Res. Biogeosci.* **111**
- Grömping U 2015 Variable importance in regression models *Wiley Interdiscip. Rev. Comput. Stat.* **7** 137–52
- Grossiord C, Buckley T N, Cernusak L A, Novick K A, Poulter B, Siegwolf R T, Sperry J S and McDowell N G 2020 Plant responses to rising vapor pressure deficit *New Phytol.* **226** 1550–66
- Hantson S et al 2016 The status and challenge of global fire modelling *Biogeosciences* **13** 3359–75
- Hantson S, Kelley D I, Arneth A, Harrison S P, Archibald S, Bachelet D, Forrest M, Hickler T, Lasslop G and Li F 2020 Quantitative assessment of fire and vegetation properties in simulations with fire-enabled vegetation models from the Fire Model Intercomparison Project *Geosci. Model Dev.* **13** 3299–318
- Hantson S, Pueyo S and Chuvieco E 2015 Global fire size distribution is driven by human impact and climate *Glob. Ecol. Biogeogr.* **24** 77–86
- Hantson S, Pueyo S and Chuvieco E 2016 Global fire size distribution: from power law to log-normal *Int. J. Wildland Fire* **25** 403–12
- Harrison S P, Prentice I C, Bloomfield K J, Dong N, Forkel M, Forrest M, Ningthoujam R K, Pellegrini A, Shen Y and Baudena M 2021 Understanding and modelling wildfire regimes: an ecological perspective *Environ. Res. Lett.* **16** 125008
- Hollingsworth T N, Johnstone J F, Bernhardt E L and Chapin F S III 2013 Fire severity filters regeneration traits to shape community assembly in Alaska's boreal forest *PLoS One* **8** e56033
- Juszczak P, Tax D and Duin R P W 2002 Feature scaling in support vector data description *Proc. ASCI 2002* (Citeseer) pp 95–102
- Kaplan J O and Lau K H-K 2021 The WGLC global gridded lightning climatology and timeseries *Earth Syst. Sci. Data Discuss.* 1–25
- Keeley J E 2009 Fire intensity, fire severity and burn severity: a brief review and suggested usage *Int. J. Wildland Fire* **18** 116–26
- Keeley J E, Pausas J G, Rundel P W, Bond W J and Bradstock R A 2011 Fire as an evolutionary pressure shaping plant traits *Trends Plant Sci.* **16** 406–11
- Keeley J E and Syphard A D 2017 Different historical fire–climate patterns in California *Int. J. Wildland Fire* **26** 253–68
- Kelley D I, Bistinas I, Whitley R, Burton C, Marthews T R and Dong N 2019 How contemporary bioclimatic and human controls change global fire regimes *Nat. Clim. Change* **9** 690–6
- Kelley D I, Prentice I C, Harrison S P, Wang H, Simard M, Fisher J B and Willis K O 2013 A comprehensive benchmarking system for evaluating global vegetation models *Biogeosciences* **10** 3313–40
- Klein Goldewijk K, Beusen A, Doelman J and Stehfest E 2017 Anthropogenic land use estimates for the Holocene–HYDE 3.2 *Earth Syst. Sci. Data* **9** 927–53
- Kloster S, Mahowald N M, Randerson J T and Lawrence P J 2012 The impacts of climate, land use, and demography on fires during the 21st century simulated by CLM-CN *Biogeosciences* **9** 509–25
- Knorr W, Arneth A and Jiang L 2016 Demographic controls of future global fire risk *Nat. Clim. Change* **6** 781–5
- Knorr W, Kaminski T, Arneth A and Weber U 2014 Impact of human population density on fire frequency at the global scale *Biogeosciences* **11** 1085–102
- Krebs P, Pezzatti G B, Mazzoleni S, Talbot L M and Conedera M 2010 Fire regime: history and definition of a key concept in disturbance ecology *Theory Biosci.* **129** 53–69
- Kuhn-Régner A, Voulgarakis A, Nowack P, Forkel M, Prentice I C and Harrison S P 2021 The importance of antecedent vegetation and drought conditions as global drivers of burnt area *Biogeosciences* **18** 3861–79
- Kumar S S, Roy D P, Boschetti L and Kremens R 2011 Exploiting the power law distribution properties of satellite fire radiative power retrievals: a method to estimate fire radiative energy and biomass burned from sparse satellite observations *J. Geophys. Res. Atmos.* **116** D19
- Larsen W A and McCleary S J 1972 The use of partial residual plots in regression analysis *Technometrics* **14** 781–90
- Lasslop G, Hantson S and Kloster S 2015 Influence of wind speed on the global variability of burned fraction: a global fire model's perspective *Int. J. Wildland Fire* **24** 989–1000
- Laurent P, Mouillot F, Moreno M V, Yue C and Ciais P 2019 Varying relationships between fire radiative power and fire size at a global scale *Biogeosciences* **16** 275–88
- Laurent P, Mouillot F, Yue C, Ciais P, Moreno M V and Nogueira J M P 2018 Data descriptor: FRY, a global database of fire patch functional traits derived from space-borne burned area products *Sci. Data* **5** 1–12
- Lehsten V, Harmand P, Palumbo I and Arneth A 2010 Modelling burned area in Africa *Biogeosciences* **7** 3199–214
- Li W, MacBean N, Ciais P, Defourny P, Lamarche C, Bontemps S, Houghton R A and Peng S 2018 Gross and net land cover changes in the main plant functional types derived from the annual ESA CCI land cover maps (1992–2015) *Earth Syst. Sci. Data* **10** 219–34
- Luo R, Hui D, Miao N, Liang C and Wells N 2017 Global relationship of fire occurrence and fire intensity: a test of intermediate fire occurrence–intensity hypothesis *J. Geophys. Res. Biogeosci.* **122** 1123–36
- McCullagh P and Nelder J A 1989 *Generalized Linear Models* 2nd edn (New York: Chapman and Hall)
- McFadden D 1974 Conditional logit analysis of qualitative choice behavior *Frontiers in Econometrics* ed P Zarembka (New York: Academic)
- Meijer J R, Huijbregts M A J, Schotten K C G J and Schipper A M 2018 Global patterns of current and future road infrastructure *Environ. Res. Lett.* **13** 064006
- Nelder J A and Wedderburn R W M 1972 Generalized linear models *J. R. Stat. Soc. A* **135** 370–84

- O'Brien R M 2007 A caution regarding rules of thumb for variance inflation factors *Qual. Quant.* **41** 673–90
- Park Williams A et al 2013 Temperature as a potent driver of regional forest drought stress and tree mortality *Nat. Clim. Change* **3** 292–7
- Pausas J G 2004 Changes in fire and climate in the eastern Iberian Peninsula (Mediterranean basin) *Clim. Change* **63** 337–50
- Pausas J G 2015 Bark thickness and fire regime *Funct. Ecol.* **29** 315–27
- Pausas J G and Keeley J E 2009 A burning story: the role of fire in the history of life *BioScience* **59** 593–601
- Pausas J G and Keeley J E 2021 Wildfires and global change *Front. Ecol. Environ.* **19** 387–95
- Pausas J G, Pratt R B, Keeley J E, Jacobsen A L, Ramirez A R, Vilagrosa A, Paula S, Kaneakua-Pia I N and Davis S D 2016 Towards understanding resprouting at the global scale *New Phytol.* **209** 945–54
- Pausas J G and Ribeiro E 2013 The global fire–productivity relationship *Glob. Ecol. Biogeogr.* **22** 728–36
- Pausas J G and Ribeiro E 2017 Fire and plant diversity at the global scale *Glob. Ecol. Biogeogr.* **26** 889–97
- Pfeiffer M, Spessa A and Kaplan J O 2013 A model for global biomass burning in preindustrial time: LPJ-LMfire (v1. 0) *Geosci. Model Dev.* **6** 643–85
- Poulter B, MacBean N, Hartley A, Khlystova I, Arino O, Betts R, Bontemps S, Boettcher M, Brockmann C and Defourny P 2015 Plant functional type classification for earth system models: results from the European Space Agency's Land Cover Climate Change Initiative *Geosci. Model Dev.* **8** 2315–28
- Povak N A, Hessburg P F and Salter R B 2018 Evidence for scale-dependent topographic controls on wildfire spread *Ecosphere* **9** e02443
- Rabin S S et al 2017 The Fire Modeling Intercomparison Project (FireMIP), phase 1: experimental and analytical protocols with detailed model descriptions *Geosci. Model Dev.* **10** 1175–97
- Ramo R, Roteta E, Bistinas I, van Wees D, Bastarrika A, Chuvieco E and van der Werf G R 2021 African burned area and fire carbon emissions are strongly impacted by small fires undetected by coarse resolution satellite data *Proc. Natl. Acad. Sci. U.S.A.* **118**
- Randerson J T, Chen Y, Wiggins E B, Hantson S, Andela N, Morton D C, Hall J, Giglio L and van der Werf G 2018 Development of the Global Fire Emissions Database (GFED): toward reconciliation of top-down and bottom-up constraints on fire contributions to variability and trends in carbonaceous aerosol *AGU Fall Meeting Abstracts 2018* pp A41E–01
- Rogers B M, Balch J K, Goetz S J, Lehmann C E R and Turetsky M 2020 Focus on changing fire regimes: interactions with climate, ecosystems, and society *Environ. Res. Lett.* **15** 030201
- Roteta E, Bastarrika A, Padilla M, Storm T and Chuvieco E 2019 Development of a Sentinel-2 burned area algorithm: Generation of a small fire database for sub-Saharan Africa *Remote Sens. Environ.* **222** 1–17
- Rothermel R C 1972 *A Mathematical Model for Predicting Fire Spread in Wildland Fuels* (United States: Intermountain Forest & Range Experiment Station, Forest Service)
- Sappington J M, Longshore K M and Thompson D B 2007 Quantifying landscape ruggedness for animal habitat analysis: a case study using bighorn sheep in the Mojave Desert *J. Wildl. Manage.* **71** 1419–26
- Schielzeth H 2010 Simple means to improve the interpretability of regression coefficients *Methods Ecol. Evol.* **1** 103–13
- Sheehan T, Bachelet D and Ferschweiler K 2015 Projected major fire and vegetation changes in the Pacific Northwest of the conterminous United States under selected CMIP5 climate futures *Ecol. Modell.* **317** 16–29
- Shiffler R E 1988 Maximum Z scores and outliers *Am. Stat.* **42** 79–80
- Sitnov S A and Mokhov I I 2018 A comparative analysis of the characteristics of active fires in the boreal forests of Eurasia and North America based on satellite data *Izv. Atmos. Ocean. Phys.* **54** 966–78
- Stocker B D, Wang H, Smith N G, Harrison S P, Keenan T F, Sandoval D, Davis T and Prentice I C 2020 P-model v1. 0: an optimality-based light use efficiency model for simulating ecosystem gross primary production *Geosci. Model Dev.* **13** 1545–81
- Sugihara N G, van Wagtenonk J W and Fites-Kaufman J 2006 Fire as an ecological process *Fire in California's Ecosystems* (Berkeley, CA: University of California Press) pp 58–74
- Tavşanoğlu Ç and Pausas J G 2018 A functional trait database for Mediterranean Basin plants *Sci. Data* **5** 180135
- Teckentrup L, Harrison S P, Hantson S, Heil A, Melton J R, Forrest M, Li F, Yue C, Arneeth A and Hickler T 2019 Response of simulated burned area to historical changes in environmental and anthropogenic factors: a comparison of seven fire models *Biogeosciences* **16** 3883–910
- Viedma O, Angeler D G and Moreno J M 2009 Landscape structural features control fire size in a Mediterranean forested area of central Spain *Int. J. Wildland Fire* **18** 575–83
- Wirth C 2005 Fire regime and tree diversity in boreal forests: implications for the carbon cycle *Forest Diversity and Function* (Berlin: Springer) pp 309–44
- Wooster M J, Roberts G, Perry G L W and Kaufman Y J 2005 Retrieval of biomass combustion rates and totals from fire radiative power observations: FRP derivation and calibration relationships between biomass consumption and fire radiative energy release *J. Geophys. Res. Atmos.* **110** D24
- Wooster M J and Zhang Y H 2004 Boreal forest fires burn less intensely in Russia than in North America *Geophys. Res. Lett.* **31** 20
- Wu C, Venevsky S, Sitch S, Mercado L M, Huntingford C and Staver A C 2021 Historical and future global burned area with changing climate and human demography *One Earth* **4** 517–30
- Yue C et al 2014 Modelling the role of fires in the terrestrial carbon balance by incorporating SPITFIRE into the global vegetation model ORCHIDEE—part 1: simulating historical global burned area and fire regimes *Geosci. Model Dev.* **7** 2747–67